

HARTREE-FOCK-BOGOLIUBOV FOR DEFORMED NEUTRON-RICH NUCLEI

NAOKI TAJIMA

Department of Basic Science, University of Tokyo, Komaba,
153-8902, Japan
E-mail: tajima@nt1.c.u-tokyo.ac.jp

Abstract

The two-basis method to solve the HFB for deformed nuclei in coordinate space is examined concerning the precision of the density tail. Small cutoff energies are shown to give rise to ripples in the tail, whose wave length corresponds to the cutoff momentum. More precise solutions require higher cutoff energies, which result in HFB matrices of larger dimensions. To circumvent the difficulty of the large dimension, we employ another method to solve the HFB—the natural-orbital method introduced originally for spherical nuclei—to apply it to deformed nuclei. The method can be successfully implemented with a three-dimensional Cartesian mesh representation.

1 Introduction

In neutron-rich nuclei, the effects of continuum states on the pairing correlation are expected to play an important role. As for nuclei near the neutron drip line, it is obvious that the continuum states are strongly involved in the pairing correlation because the Fermi level λ_n and the pairing gap Δ_n have similar sizes $\sim \pm 1$ MeV. The effect of such a continuum-state pairing may be so strong that the neutron drip line can be pushed outward by several nuclei.[1]

For nuclei with $\lambda_n \gtrsim -5$ MeV, too, the continuum states should be taken into account explicitly because the pairing-active space for HFB calculations should be larger than one major shell, i.e., $\epsilon_{\text{cut}} > \lambda + \hbar\omega$, in order to take into account a correct size of shell effects.

The pairing correlation has been treated usually in the BCS approximation, which relies on an assumption that the pair-scattering matrix elements $\langle \psi_i \psi_i | V_p | \psi_j \psi_j \rangle$ do not depend on the form of the wavefunctions ψ_i and ψ_j , e.g. a constant. This assumption results in a situation that the nucleus is surrounded by unphysical dilute neutron gas when $\epsilon_{\text{cut}} > 0$. Therefore, to include the positive energy states in the pairing correlation, one needs to switch from the HF(Hartree-Fock)+BCS to the Hartree-Fock-Bogoliubov (HFB) scheme in coordinate space.

So far, several methods have been presented to solve the HFB equation. For spherical nuclei, there are three methods:

- 1) Radial differential equations (Dobaczewski et al., 1984),[2]

- 2) Finite-element method for finite-range pairing forces (Ring et al., 1997),[3]
- 3) Natural-orbital representation (Reinhard et al, 1997).[4]

For deformed nuclei, two methods have been presented. Although spherical cases can be solved easily with present computers, deformed cases in coordinate space are still a challenge.

- 4) Diagonalization in the harmonic-oscillator basis (Gogny et al., 1980),[5]
- 5) Two-basis method (Heenen et al., 1994).[6, 7, 8]

In this paper, we describe the formulations in the subsequent two sections and then study two subjects: First, in section 4, we examine the two-basis method concerning the precision of the low-density tail at large radius as a function of the cutoff energy, i.e., the number of HF orbitals included in the diagonalization. We show that more precise solutions require higher cutoff energies, which result in HFB matrices of larger dimensions. Second, in section 5, we test the natural-orbital method for deformed cases in a three-dimensional (3D) Cartesian mesh representation.

2 HFB in coordinate space

In this section, we formulate the HF and the HFB in the coordinate-space representation in order to elucidate a difficulty of the HFB and to suggest its possible solution in terms of the natural-orbital representation. For the sake of simplicity, in this section, we consider only one kind of nucleons and designate the number of nucleons by N . The spin of a nucleon is represented by s .

2.1 HF

In the HF, one should minimize $\langle \Psi | H | \Psi \rangle$ for single Slater-determinant states,

$$|\Psi\rangle = \prod_{i=1}^N a_i^\dagger |0\rangle, \quad (1)$$

$$a_i^\dagger = \sum_s \int d\vec{r} \psi_i(\vec{r}, s) a_{\vec{r}s}^\dagger \quad : \text{single-particle state}, \quad (2)$$

by varying $\{\psi_i\}_{i=1,\dots,N}$ under orthonormality conditions $\langle \psi_i | \psi_j \rangle = \delta_{ij}$.

2.2 HFB

In the HFB, the state takes the following form,

$$|\Psi\rangle = \prod_{i=1}^{\#\text{basis}} b_i |0\rangle, \quad (3)$$

$$b_i = \sum_s \int d\vec{r} \left\{ \phi_i^*(\vec{r}, s) a_{\vec{r}s} + \varphi_i(\vec{r}, s) a_{\vec{r}s}^\dagger \right\} \quad : \text{quasi-particle state}, \quad (4)$$

where “#basis” is the number of basis states of the employed representation: For a 3D-mesh representation,[9] it is the number of the mesh points (times four when spin-orbit potentials are included) and typically 10^4 - 10^5 . One should vary $\{\phi_i, \varphi_i\}_{i=1,\dots,\#\text{basis}}$ under appropriate orthonormality conditions.

The essential difference between the HF and the HFB is that one has to consider only $N \sim 10^2$ wavefunctions in the former while one has to treat explicitly as many single-particle wavefunctions as the number of the basis in the latter.

2.3 HFB with the two-basis method

In this method, the HFB equation is solved by diagonalizing the HFB matrix in a single-particle basis $\{\psi_i\}_{i=1,\dots,K}$ consisting of the eigenstates of the mean-field hamiltonian h (excluding the pairing potential): $h\psi_i = \epsilon_i\psi_i$. The number of the basis, K , is determined by a cutoff energy ϵ_{cut} as $\epsilon_1 \leq \dots \leq \epsilon_K \leq \epsilon_{\text{cut}} \leq \epsilon_{K+1} \leq \dots$. We will show in section 4 that $K \gg N$ to obtain high-precision density tails.

Figure 1

Figure 1: Schematic picture to explain the different number of single-particle states necessary to express the HFB ground state between the two-basis and the natural-orbital methods.

2.4 HFB in natural-orbital basis

Owing to the Bloch-Messiah theorem, the state (3) can be expressed as,

$$|\Psi\rangle = \prod_{i=1}^{\#\text{basis}} (u_i + v_i a_i^\dagger a_i^\dagger) |0\rangle, \quad (5)$$

$$a_i^\dagger = \sum_s \int d\vec{r} \psi_i(\vec{r}, s) a_{\vec{r}s}^\dagger \quad : \text{natural orbital (canonical basis)}. \quad (6)$$

One should vary $\{\psi_i, u_i\}_{i=1,\dots,\#\text{basis}}$ under constraints for orthonormality,

$$\langle \psi_i | \psi_j \rangle = \delta_{ij} \quad (1 \leq i \leq j \leq \#\text{basis}), \quad (7)$$

and for the expectation value of the number of nucleons, $2 \sum_{i=1}^K v_i^2 = N$.

Reinhard et al. regard the advantage of the representation (5) over (3) to be that one has to consider only a single set of wavefunctions $\{\psi_i\}$ unlike a double set $\{\phi_i, \varphi_i\}$.[4] However, we expect more benefit from the natural-orbital representation. Namely, i may be truncated as $i \leq K = \mathcal{O}(N) \ll \#\text{basis}$ to a very good approximation. It is because ψ_i should be a localized function while the orthogonality does not allow many wavefunctions to exist in the vicinity of the nucleus. This situation is illustrated in Fig. 1. For 3D-mesh representations, $\#\text{basis}$ is proportional to the volume of the cavity (box) while K is proportional to the volume of the nucleus. The latter is 10^1 - 10^2 times as small as the former.

3 HFB with density-dependent zero-range forces

3.1 Interaction

We employ density-dependent zero-range interactions in the rest of this paper for the sake of simplicity. There will not be essential differences in the formulation if we use the full-form Skyrme force. The force is expressed in the parameterization of the Skyrme force as,

$$V(\vec{r}_1, s_1; \vec{r}_2, s_2) = \left(t_0 + \frac{1}{6} t_3 \rho (\vec{r}_1)^\alpha \right) \delta(\vec{r}_1 - \vec{r}_2). \quad (8)$$

We adopt $t_0 = -1099$ MeV fm³, $t_3 = 17624$ MeV fm^{3+3α}, and $\alpha = 0.98$ (it is not 1 only for the sake of a test of the code) when the force is used to construct the mean-field (HF) potential.[10] We use a different strength to make the pairing potential. We express the force in the parameterization of Ref.[11]:

$$V_p(\vec{r}_1, s_1; \vec{r}_2, s_2) = v_p \frac{1 - P_\sigma}{2} \left(1 - \frac{\rho(\vec{r}_1)}{\rho_c} \right) \delta(\vec{r}_1 - \vec{r}_2). \quad (9)$$

We use $\rho_c = 0.32$ fm⁻³ (to roughly vanish the volume-changing effect[11]).

3.2 Hamiltonian density

For the sake of simplicity, we treat $N=Z$ nuclei without Coulomb interaction in the rest of this paper. Then, the state of the nucleus is expressed as,

$$|\Psi\rangle = \prod_{i=1}^K \left(u_i + v_i a_i^\dagger a_i^\dagger \right)_{\text{proton}} \left(u_i + v_i a_i^\dagger a_i^\dagger \right)_{\text{neutron}} |0\rangle. \quad (10)$$

With the interactions (8) and (9), the total energy for state (10) is written as,

$$E = \langle \Psi | H | \Psi \rangle = \int \mathcal{H}(\vec{r}) d\vec{r}, \quad (11)$$

$$\mathcal{H} = \frac{\hbar^2}{2m} \tau + \frac{3}{8} t_0 \rho^2 + \frac{1}{16} t_3 \rho^{2+\alpha} + \frac{1}{8} v_p \left(1 - \frac{\rho}{\rho_c} \right) \tilde{\rho}^2, \quad (12)$$

where τ is the kinetic energy density,

$$\rho(\vec{r}) = 4 \sum_{i=1}^K v_i^2 |\psi_i(\vec{r})|^2, \quad \tilde{\rho}(\vec{r}) = 4 \sum_{i=1}^K u_i v_i |\psi_i(\vec{r})|^2. \quad (13)$$

The stationary condition $\delta \mathcal{H} = 0$ leads to a mean-field and a pairing potentials:

$$h = -\frac{\delta E}{\delta \rho} = \frac{\hbar^2}{2m} \vec{\nabla}^2 + \frac{3}{4} t_0 \rho + \frac{2+\alpha}{16} t_3 \rho^{1+\alpha} - \frac{v_p}{8\rho_c} \tilde{\rho}^2, \quad (14)$$

$$\tilde{h} = \frac{\delta E}{\delta \tilde{\rho}} = \frac{1}{4} v_p \left(1 - \frac{\rho}{\rho_c} \right) \tilde{\rho}. \quad (15)$$

4 Test of the accuracy of the two-basis method for HFB

We have developed from scratch an HFB program for spherical cases based on the two-basis method explained in sect. 2.3. It is used to examine the precision of the low-density tail at large radius as a function of the cutoff energy ϵ_{cut} .

In Fig. 2 we show the density profiles for $(Z, N) = (38, 68)$ calculated with the Braghin-Vautherin force[12] and $v_p = -400$ MeV. One can see that (i) The density is localized with accuracy $\sim 10^{-6}$ fm $^{-3}$. (ii) The cutoff makes ripples in the tail. The wave-length of the ripples agrees with $2\pi\hbar(2m\epsilon_{\text{cut}})^{-1/2}$, i.e., half of the de Broglie wavelength for ϵ_{cut} .

Figure 2

Figure 2: Density profiles of HF and two-basis HFB solutions.

To obtain a more precise density tail, one has to increase ϵ_{cut} , which results in an increase of K , the number of single-particle wavefunctions to be considered explicitly. K increases only slowly as $\epsilon_{\text{cut}}^{1/2}$ for spherical case for each angular momentum, while it grows rapidly as $\epsilon_{\text{cut}}^{3/2}$ for deformed case. The rapid grow of the latter case makes the two-basis method practically inapplicable to deformed nuclei because the bottle-necks in computation of mean-field methods on 3D meshes are the parts which spend computation time proportional to K^2 like the orthogonalization. Therefore, one need a different method to solve the HFB for deformed nuclei with enough high cutoff energies.

5 Implementation of the natural-orbital HFB method on 3D mesh

The natural-orbital method explained in sect. 2.4 was originally introduced for spherical nuclei.[4] We have implemented the method to treat deformed nuclei in a 3D-mesh representation.

First, let us present a summary of the formulation, which has some differences from Ref.[4] Instead of minimizing $E = \langle \Psi | H | \Psi \rangle$ with $|\Psi\rangle$ given by Eq. (10) under constraints of Eq. (7), one may introduced a Routhian R ,

$$R = E - \epsilon_{\text{Fermi}} \cdot 4 \sum_{i=1}^K v_i^2 - \sum_{i=1}^K \sum_{j=1}^K \lambda_{ij} \{ \langle \psi_i | \psi_j \rangle - \delta_{ij} \}, \quad \lambda_{ij} = \lambda_{ji}^*, \quad (16)$$

and minimize it without constraints. In the above definition, in order to make R real for the sake of convenience, K^2 Lagrange multipliers λ_{ij} obeying hermiticity are introduced instead of $\frac{1}{2}K(K+1)$ independent multipliers. Note that δ_{ij} is subtracted from $\langle \psi_i | \psi_j \rangle$ in order to treat λ_{ij} not as constants like ϵ_{Fermi} but as functionals of the wavefunctions.

Stationary conditions of R result in the following equations.

$$\frac{\partial R}{\partial v_i} = 0 \Rightarrow v_i^2 = \frac{1}{2} - \frac{1}{2} \frac{h_{ii} - \lambda}{\sqrt{(h_{ii} - \lambda)^2 + \tilde{h}_{ii}^2}}, \quad \text{assuming } \tilde{h}_{ii} \leq 0, \quad (17)$$

$$\frac{\delta R}{\delta \psi_i^*} = 0 \Rightarrow \mathcal{H}_i \psi_i - \sum_{j=1}^K \lambda_{ij} \psi_j - \sum_{j=1}^K \sum_{k=1}^K \frac{\delta \lambda_{jk}}{\delta \psi_i^*} \{ \langle \psi_j | \psi_k \rangle - \delta_{jk} \} = 0, \quad (18)$$

$$\mathcal{H}_i = v_i^2 h + u_i v_i \tilde{h}. \quad (19)$$

For HF, the orthogonalization conditions are easily realized because ψ_i are eigenstates of the same hermite operator h and thus are orthogonal at the solution: The orthogonalization procedure is needed only because the orthogonality is unstable. On the other

hand, for the natural-orbital HFB method, the orthogonalization is essential because the single-particle hamiltonians \mathcal{H}_i differs from state to state. Therefore, the determination of the explicit functional form of λ_{ij} is the most important part of the method. Reinhard et al. have proposed

$$\lambda_{ij} = \frac{1}{2} \langle \psi_j | (\mathcal{H}_i + \mathcal{H}_j) | \psi_i \rangle. \quad (20)$$

We can justify their choice as follows: From the requirement that Eq. (18) must hold at the solution (where $\langle \psi_i | \psi_j \rangle = \delta_{ij}$), one deduces,

$$\lambda_{ij} = \langle \psi_j | \mathcal{H}_i | \psi_i \rangle \quad \text{at the solution.} \quad (21)$$

Eqs. (20) and (21) are equivalent at the solution because λ_{ij} is defined to be hermite. Since this hermiticity must hold at any points, one should not adopt Eq. (21) but Eq. (20). Because what is needed is Eq. (21) and the hermiticity, one may use more complex forms like,

$$\lambda_{ij} = \frac{1}{2} \langle \psi_j | (\mathcal{H}_i + \mathcal{H}_j) | \psi_i \rangle \left\{ 1 + f_2 (\langle \psi_j | \mathcal{H}_i | \psi_i \rangle - \langle \psi_j | \mathcal{H}_j | \psi_i \rangle)^2 \right\}, \quad (22)$$

where f_2 is a parameter to maximize the convergence speed.

To obtain the HFB solutions in the natural-orbital formalism, one can utilize the gradient method, which includes the imaginary-time evolution method:

$$\psi_i \rightarrow \psi_i - \Delta\tau \frac{\delta R}{\delta \psi_i^*} \quad (23)$$

We have developed a 3D-mesh natural-orbital HFB program from scratch according to the above formulation. First of all, we test the feasibility of the method for ^{40}Ca . The wavefunctions are expressed with $39 \times 39 \times 39$ mesh points with mesh spacing of 0.8 fm. Note that the requirement of precision is higher for HFB than for HF because one has to treat larger momentum components than the Fermi momentum in HFB. We employed the 17-point finite-difference approximation to the Laplacian. The vanishing boundary conditions are imposed on the boundary (0th and 40th mesh points) and the wavefunctions are anti-symmetrically reflected in the boundary to apply the finite-difference formula. We considered $K = 20$ natural orbitals, which can contain 80 ($= 2 \times A$) nucleons.

Figure 3

Figure 3: Convergence of HF and HFB in the natural-orbital method.

We show an example of the convergence history in Fig. 3. In this calculation, we set $f_2 = 0$ in Eq. (22) and $\Delta\tau = 10^{-24}$ sec in Eq. (23). We neglect $\delta\lambda/\delta\psi^*$ in Eq. (18). Instead, at every 50 steps, $\{\psi_i\}$ are Gram-Schmidt orthogonalized in the ascending order of h_{ii} and then the HFB hamiltonian is diagonalized in the basis to renew $\{\psi_i, v_i\}$.

In the left-hand portion, the error of Eq. (18), i.e., $\max_{i=1,\dots,K} |\mathcal{H}_i \psi_i - \sum_j \lambda_{ij} \psi_j|$ are plotted versus the evolution step. The corresponding quantity for HF, $\max_{i=1,\dots,A/4} |h \psi_i - \langle \psi_i | h | \psi_i \rangle \psi_i|$, is also plotted. The figure demonstrates that one can indeed obtain HFB solutions with the natural-orbital HFB method in the 3D-mesh representation. We obtained

similar convergence curves for the error of the orthogonality and for the inconsistency between the potential and the densities. The right-hand portion shows the error of the total energy (estimated as the difference of the total energy from the convergent value), which also shows an exponential convergence pattern.

The speed of the convergence is, however, about ten times as slow as the HF case. We are now trying to improve the convergence speed, the stability of the evolution, and the robustness of the method.

6 Influence of pairing correlation on deformation

As examples of the applications of our natural-orbital HFB program, we show in Fig. 4 the change of shape due to pairing correlation. The root-mean-square values of x , y , and z are plotted as functions of the strength of the pairing interaction v_p for ^{32}S and ^{60}Zn . Both nuclei are triaxial when the pairing correlation is off (pairing gap $\Delta = 0$). However, as soon as the pairing correlation sets in, the axial symmetry is restored.

The pairing correlation does not always restore symmetric shapes but sometimes break a symmetry present without pairing: For ^{60}Zn , the expectation value of $\frac{1}{2}(1 - \tau_z)Y_{30}$ is zero before the pairing sets in while it is about half the Weiskopf unit when the pairing correlation is present.

Figure 4

Figure 4: Triaxiality of HFB solutions versus the strength of the pairing interaction.

Acknowledgments

The author thanks to Prof. J. Dobaczewski, Prof. P.-H. Heenen, Prof. D. Brink and Prof. N. Onishi for discussions during and after the symposium.

References

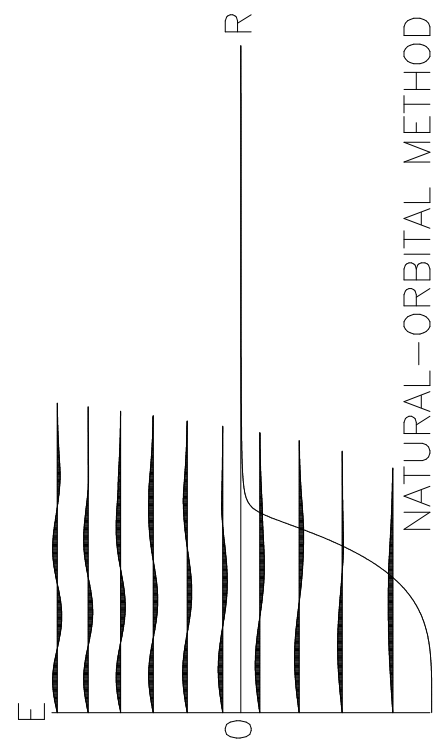
- [1] J. Dobaczewski, Nazarewicz et al., Phys. Rev. **C53** (1996) 2809.
- [2] J. Dobaczewski, Flocard and Treiner, Nucl. Phys. **A422** (1984) 103.
- [3] W. Poeschl, Vretenar, Lalazissis et al., Phys. Rev. Lett. **79** (1997) 3841.
- [4] P.-G. Reinhard, Bender, Rutz and Maruhn, Z. Phys. **A358** (1997) 277.
- [5] J. Dechargé and D. Gogny, Phys. Rev. **C21** (1980) 1568.
- [6] B. Gall, Bonche, Dobaczewski et al., Z. Phys. **A348** (1994) 183.
- [7] J. Terasaki, Heenen, Flocard and Bonche, Nucl. Phys. **A600** (1996) 371.

- [8] J. Terasaki, Flocard, Heenen and Bonche, Nucl. Phys. **A621** (1997) 706.
- [9] P. Bonche, H. Flocard, Heenen et al., Nucl. Phys. **A443** (1985) 39.
- [10] S.E. Koonin, Phys. Lett. **B61** (1976) 227.
- [11] N. Tajima, P. Bonche, H. Flocard et al., Nucl. Phys. **A551** (1993) 434.
- [12] F.L. Braghin and D. Vautherin, Phys. Lett. **B333** (1994) 289.

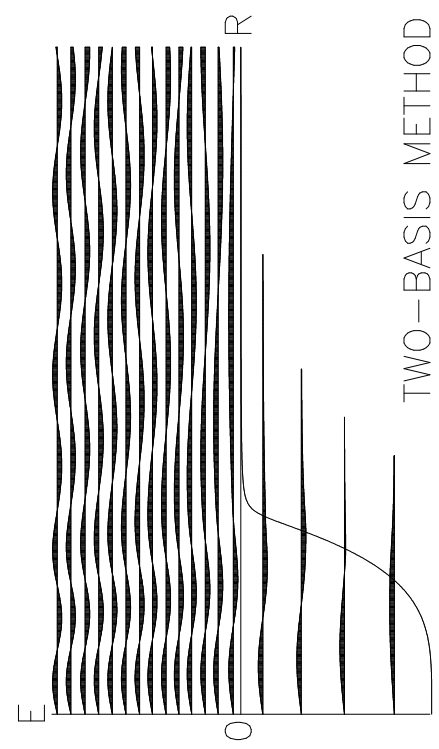
This paper has been published in the proceedings of the XVII RCNP international symposium on Innovative Computational Methods in Nuclear Many-Body Problems –Towards a new generation of physics in finite quantum systems– (INNOCOM97), Osaka, Japan, November 10-15, 1997, edited by H. Horiuchi, M. Kamimura, H. Toki, F. Fujiwara, M. Matsuo, and Y. Sakuragi, (1998) World Scientific (Singapore), pp. 343-351.

The present address of the author is:

Department of Applied Physics, Fukui University,
Bunkyo 3-9-1, Fukui, 910-8507, Japan
E-mail: tajima@quantum.apphy.fukui-u.ac.jp



NATURAL-ORBITAL METHOD



TWO-BASIS METHOD

